Journal of Scientific & Industrial Research
Vol. 85, March 2026, pp. 252-265
DOI: 10.56042/jsir.v85i3.13210

A Study on Sensitivity Performance of CMOS-MEMS Pressure Sensors utilizing Split Channel MOSFET Structures

Kalpana Gogoi[1]*, Menuvolu Tetseo[1], Gaurav Kumar[1], Pradeep Kumar Rathore[1], Shashi Kumar[2], Peesapati Rangababu[3], Jaspreet Singh[4] & Brishbhan Singh Panwar[5]

[1]Department of Electronics and Communication Engineering, National Institute of Technology Meghalaya, Shillong 793 003, India

[2]Numelo Technologies Pvt. Ltd. (A startup of IIT Bombay), Indian Institute of Technology Bombay, Mumbai, 400 076, India

[3]Department of Electronics and Communication Engineering, Indian Institute of Information Technology Design and Manufacturing, Kurnool, 518 008, India

[4]Semi-Conductor Laboratory, Ministry of Electronics and Information Technology, Government of India, Mohali, 160 071, India

[5]Department of Electrical, Electronics & Communication Engineering, Dehradun Institute of Technology (DIT) University, Mussoorie, 248 009, India

Received 17 August 2024; revised 10 March 2026; accepted 07 April 2026

The paper presents a simulation study on the sensitivity performance of CMOS-MEMS pressure sensors utilizing the Split channel MOSFET structures. These pressure sensors have been designed as split circular curved and split square curved channel MOSFETs integrated on corresponding silicon based circular and square diaphragms. These pressure sensors operate using the piezoresistive effect of MOSFET as a transduction mechanism, referred to as piezo-MOS. The research has been carried out using n-MOS, p-MOS, and CMOS (integrated p-MOS and n-MOS) current mirror circuits. Each circuit has been individually integrated with both diaphragm geometries. The proposed pressure sensors were redesigned using SCL 180 nm CMOS technology, with a 100 µm channel width and 10 µm channel length. The piezo-MOS structure has been split into four segments, resulting in a current mirror integrated split curved channel MOSFET pressure sensor. The mechanical properties of the proposed pressure sensors have been studied using the finite element analysis solver, COMSOL Multiphysics software. The circuit characteristics have been evaluated using Tanner T-Spice. The external pressure ranging from 0 kPa to 450 kPa has been applied to the pressure sensors. The sensitivities of n-MOS, p-MOS, and CMOS (integrated p-MOS and n-MOS) current mirrors, for Split circular curved channel pressure sensor, have been obtained as 122.051, 0.249, and 377.611 mV/MPa, respectively. Similarly, for the Split square curved channel, it has been obtained as 138.821, 0.401, and 492.250 mV/MPa, respectively, for the corresponding readout circuits. The sensitivity variation over different temperature ranges has also been studied and compared for the proposed pressure sensors. Enhanced sensitivity and compatibility with CMOS technology could make the proposed pressure sensors suitable for the next-generation pressure sensing devices.

Keywords: Circuit characteristics, Current mirror, Finite element analysis, Piezoresistive effect, Split channel MOSFET

Introduction

The rapidly growing MEMS (Micro-Electro-Mechanical-System) industry and the demand for pressure sensors in recent years have developed many devices and standard smart pressure sensors utilizing the MEMS technology.[1,2] Recently, it has been observed that researchers worldwide have been showing significant interest in the integration of MEMS and CMOS technology for creating micro-scaled sensors.[3] These integrated devices or pressure sensors enable the fabrication of mechanical sensing microstructure with CMOS-integrated microelectronic circuits in a single-chip package.[3–5] The miniaturization of micro pressure sensors leads to cost reduction, enhanced performance, improved accessibility, space-saving, and low energy consumption.[6,7] MEMS pressure sensors are the first device fabricated on silicon utilizing the piezoresistive effect and are being commercialized.[2] Nowadays, it is being frequently used in the field of medical diagnosis due to advanced treatments. Also, in the past few decades, miniaturized pressure sensors were developed with smaller chips in sizes that give precise measurements, finer resolutions, harsh environments adaptability, and are easy to handle. Some MEMS-based pressure sensors that are pivotal in medical healthcare are Intraocular pressure

*Author for Correspondence
E-mail: gogoikalpana22@gmail.com

monitoring for detecting Glaucoma, Digital Sphygmomanometers for blood pressure measurement, and Electrocardiogram (ECG) monitoring to detect Cardiovascular Disease (CVD), and measuring heartbeats.[8–10]

The pressure sensors are designed using the mechanical sensing mechanisms that convert a physical form of energy into electrical energy.[11] Piezoresistive, Capacitive, Piezoelectric, and Optical are some of the sensing transduction mechanisms that are utilized in the field of Microelectro mechanical systems.[11,12] However, they come with certain limitations: In piezoresistive, piezoresistors are arranged in straightforward construction using the Wheatstone bridge configuration. But it has a major drawback in the requirement of temperature compensation circuits, because the silicon piezoresistors are sensitive to temperature and suffer from temperature cross-sensitivity.[13–15] In Capacitive, the distance between the electrodes and capacitance is inversely proportional to one another due to which it gives non-linearity output.[16–18] In piezoelectric, it is well suited for dynamic measurement and is not good for every static sensing and also its properties degrade with increasing temperature.[19,20] The optical causes the vulnerability to interference from environmental effects and bodily harm.[21]

The recent advances in technology and CMOS integration with MEMS enable the development of a MOSFET-based sensing mechanism called piezo-MOS. The mechanism leverages the piezoresistive effect of MOSFET to provide high-precision sensing.[23] It bases its hypothesis on the idea that the differences in the mobility of holes and electrons of the MOSFETs under applied pressure cause the variation in drain current and voltage in it.[23,24] The integration of the current mirror with pressure sensing structure enhances the compatibility and provides better sensitivities.[25,26] The current mirror is an extensively used circuit that provides an active load and bias current to the circuit.[22] It supports CMOS-MEMS technology for designing the scaled-down miniaturized pressure sensor. Our research team has been focusing on the development of the piezo-MOS sensing mechanism integrated with current mirror using various structural designs and patterns for extracting better and higher sensitivities.[27–29] In some of our previous works on pressure and mass sensors utilizing piezo-MOS sensing mechanisms for different shapes and dimensions, it has been observed and found to have better sensitivities.[30–33] Our team has also designed and fabricated the pressure sensing devices, utilizing the n-type and p-type MOSFET current mirror circuit.[34,35]

In this work, the pressure sensors are designed using the SCL 180 nm CMOS technology. The Split circular and square curved channel piezoresistors have been integrated on the circular and square diaphragms, respectively. Each diaphragm structure has integrated three distinct current mirror readout circuits, n-MOS, p-MOS, and CMOS (integrated p-MOS and n-MOS) independently on it. Here, the pressure-sensing mechanisms and diaphragm dimensions were assumed to be the same as in our previous work.[31] However, the piezoresistor has been split into four segments because of the changing channel dimensions and technological parameters in SCL 180 nm CMOS technology. The pressure range for these pressure sensors has been taken from 0 kPa to 450 kPa. The sensitivities to different temperature ranges have also been studied and compared. This work also includes a literature survey on the various pressure sensors and their sensitivities, including the applications of pressure sensors within 0–500 kPa input range.

Methodology: Sensor structure, Working principle, and Fabrication process flow

Structural and Theoretical model of Current Mirror integrated Split curved channel MOSFET pressure sensor

The micro pressure sensor proposed in this paper contains the silicon-based Circular and Square diaphragms. This microstructure pressure sensor has been designed in the split form of curved shaped piezoresistors embedded on circular and square diaphragms and are integrated with (a) n-MOS resistive load current mirror circuit, (b) p-MOS resistive load current mirror circuit, and (c) CMOS (integrated p-MOS and n-MOS) current mirror circuit. Here, each circuit has been integrated independently on each circular and square structure.

The circular and square Split curved channel MOSFETs integrated on circular and square diaphragms are represented in Figs. 1(a) and (b), respectively. The n-MOS resistive load current mirror readout circuit, which has two n-type MOSFETs (N1 and N2), is shown in Fig. 2(a). Here, N1 is the transistor on the substrate as reference n-MOS, and N2 is the transistor on the edges of the diaphragm as pressure-sensing n-MOS. Likewise, Fig. 2(b) shows the p-MOS resistive load current mirror readout circuit that has two p-type MOSFETs, where P1 acts

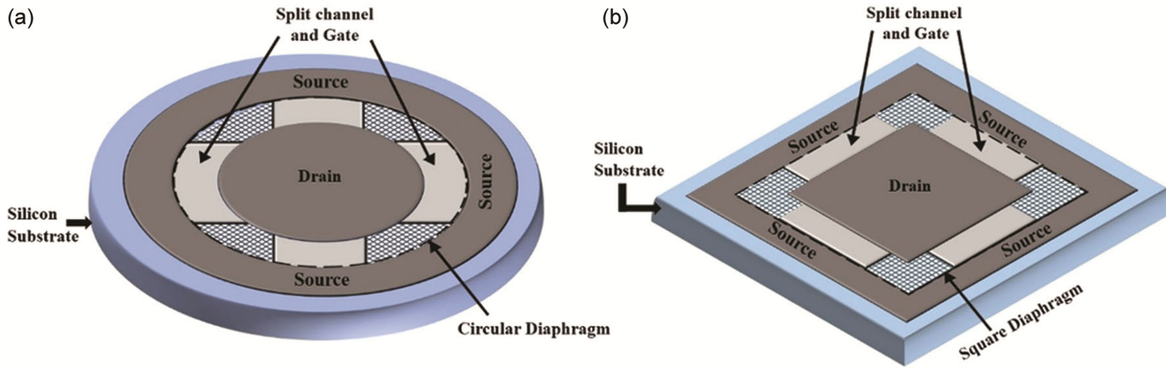

Fig. 1 — Structural model of: (a) Split curved channel circular MOSFET integrated on the circular diaphragm, and (b) Split curved channel square MOSFET integrated on the square diaphragm

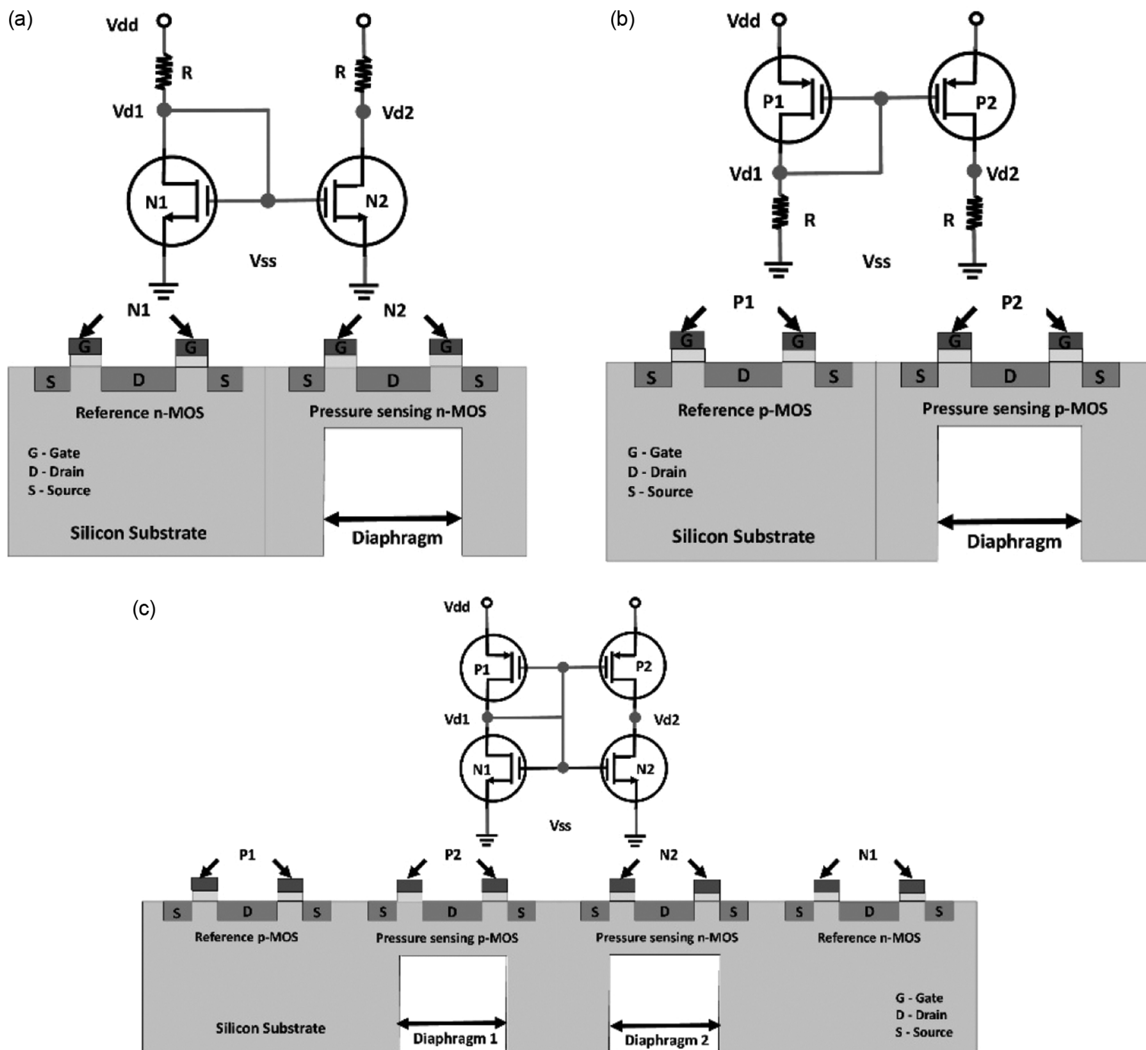

Fig. 2 — Representation of current mirror circuit on proposed micro pressure sensor: (a) n-MOS resistive load current mirror on circular and square diaphragm, (b) p-MOS resistive load current mirror on circular and square diaphragm, (c) CMOS current mirror (integrated p-MOS & n-MOS) on circular and square diaphragm

as a reference p-MOS on the substrate and P2 as a pressure-sensing p-MOS at the edges of the diaphragm. From Fig. 1, it can be observed that the Split curved channel MOSFETs are integrated on the diaphragm's fixed edge. Therefore, the proposed pressure sensors will experience the highest stress at the mid-point of the periphery of square diaphragm, and in the circular diaphragm, the highest stresses are obtained on the entire periphery of diaphragm. These micro-pressure sensors work on the principle where the application of external pressures modulates the MOSFET electron and hole mobilities, which enables the change in the drain voltage and drain current. This change occurs due to the piezoresistive effect of the MOSFET. Therefore, the output voltages are obtained from the drain terminals of N1 and N2 for the n-type MOSFET, and P1 and P2 for the p-type MOSFET.

The CMOS (integrated p-MOS and n-MOS) circuit integrated on circular and square diaphragms is presented in Fig. 2(c). This pressure sensor has two identical diaphragms (Circular or Square) as mechanical elements, and the circuit diagram has two p-type MOSFETs and two n-type MOSFETs. The transistors N1 and P1 act as reference n-MOS and reference p-MOS, respectively, whereas N2 and P2 are located at the periphery of the diaphragms and act as pressure-sensing n-MOS and pressure-sensing p-MOS, respectively. The pressure is applied on the structure, due to which there is a deformation in the diaphragm that causes changes in the mobilities in MOSFETs (N2 and P2), resulting in the variation of drain voltage and drain current of N2 and P2, thus, obtaining the output voltages from the drain terminals of MOSFETs (P1, N1 and P2, N2).

Mechanics of Diaphragm Structures

The mechanical structures are the basic elements for the construction of MEMS sensors. The proposed Current Mirror integrated Split curved channel MOSFET pressure sensors are designed on Circular and Square diaphragms. The maximum displacement (W_{max}) and Stress (T_{max}) equations under applied pressure have been studied and are utilized for the proposed micro-pressure sensors.[11]

The displacement equations for the circular and square diaphragms are given in Eqs (1) & (2). The center of the diaphragms gives maximum displacement due to the applied pressure, and therefore, the expressions are represented as:

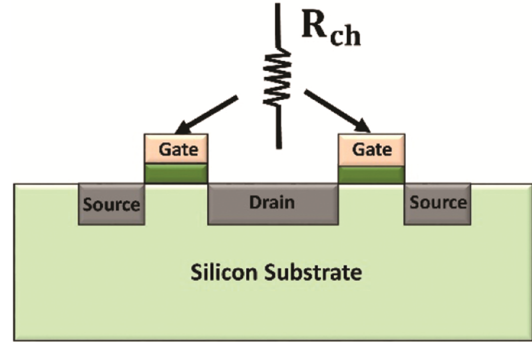

Fig. 3 — Representation of the MOSFET equivalent piezoresistor integrated on circular and square diaphragms

$$W_{max\,(Circular)} = 0.1875pa^4 \frac{(1-\nu^2)}{Eh^3} \quad \ldots (1)$$

$$W_{max\,(Square)} = 0.255pa^4 \frac{(1-\nu^2)}{Eh^3} \quad \ldots (2)$$

Due to the pressure exerted on the diaphragms, stresses are developed in them. The equations of stress for both circular and square diaphragms have been studied and utilized for the proposed micro-pressure sensors. For the Circular diaphragm, stresses are developed at the entire diaphragm edges, and for the square, stresses are formed at the center of the diaphragm edges. Therefore, they are represented as:

$$T_{max\,(Circular)} = 0.75p\frac{a^2}{h^2} \quad \ldots (3)$$

$$T_{max(Square)} = 1.02p\frac{a^2}{h^2} \quad \ldots (4)$$

where, p, a, h, E, and ν are the pressure, the diaphragm's diameter or side, thickness, Young's modulus of elasticity, and Poisson ratio, respectively.

Electrical Properties of MOSFET Sensing Pressure Sensor

The Split curved channel current mirror integrated pressure sensors have a MOSFET equivalent piezoresistor, as shown in Fig. 3. The MOS transistors allow maximum current flow and operate in the saturation region. Therefore, the drain current (I_D) in saturation and at zero pressure application is defined in Eq. (5) for both n-MOSFET and p-MOSFET.

$$I_D = \frac{1}{2}\mu C_{ox}\frac{W}{L}(V_{GS}-V_{th})^2 \quad \ldots (5)$$

In the above formula, μ is the mobility in electrons and holes of MOSFET. C_{ox} is the capacitance on gate oxide per unit area, W and L are the width and length of the channel in MOSFET. The applied voltage in the gate-source is denoted as V_{GS} and V_{th} is the threshold voltage.

The operational framework for the reported pressure sensor is that it works on the piezoresistive effect of MOSFET. Here, on applying pressure, carrier mobilities change their behavior with the changing drain current and drain voltage. Therefore, the change in the mobility of electrons and holes ($\Delta\mu/\mu$), is equivalent to the changes in channel resistance ($\Delta R_{ch}/R_{ch}$), and the equation for this is defined as:

$$\frac{\Delta\mu}{\mu} \approx -\frac{\Delta R_{Ch}}{R_{Ch}} = -\pi T \quad \dots (6)$$

Here, and T are defined as the MOSFET piezoresistive coefficient and the stresses that occurred in the MOSFET channel region, respectively. Therefore, the drain current for p-channel and n-channel under stress and applying pressure is defined in Eq. (7).

$$I_{D(Pressure)} = (\mu \pm \Delta\mu)C_{ox}\frac{W}{L}\frac{(V_{GS} - V_t)}{2} \quad \dots (7)$$

Readout Circuit for Proposed Pressure Sensors

The Split curved channel pressure sensors utilize the Current mirror (CM) configuration circuit, whose output voltages are measured in the drain terminals of the transistors and are directly related to the input applying pressure. This section introduces the effect of stress on the MOSFET for each current mirror.

pMOS and nMOS Resistive Load CM

In the pMOS and nMOS resistive load current mirror, there are two MOSFETs for both p-channel (P1 & P2) and n-channel (N1 & N2), respectively. The MOSFETs P1 and N1 of the pressure sensors are integrated in the substrate, and therefore, they are independent of stresses. Hence, it will be independent of variation in mobilities, drain current, and drain voltage, and therefore:

$$\Delta\mu_{(P1)} = \Delta\mu_{(N1)} = 0 \quad \dots (8)$$

Here, $\Delta\mu_{(P1)}$ and $\Delta\mu_{(N1)}$ are the changes in mobilities in p- and n-channel, respectively. Therefore, the drain current (I_D) and drain to source voltage (V_{DS}) are represented as:

For p-MOSFET:

$$I_{D(P1)} = \{\mu_{(P1)} \pm \Delta\mu_{(P1)}\}C_{ox}\frac{W}{L}\frac{(V_{GS} - V_t)}{2} = \mu_{(P1)}C_{ox}\frac{W}{L}\frac{(V_{GS} - V_t)}{2} \quad \dots (9)$$

$$V_{DS(P1)} = V_{DD} - I_{D(P1)}R_D \quad \dots (10)$$

For n-MOSFET:

$$I_{D(N1)} = \{\mu_{(N1)} \pm \Delta\mu_{(N1)}\}C_{ox}\frac{W}{L}\frac{(V_{GS} - V_t)}{2} = \mu_{(N1)}C_{ox}\frac{W}{L}\frac{(V_{GS} - V_t)}{2} \quad \dots (11)$$

$$V_{DS(N1)} = V_{DD} - I_{D(N1)}R_D \quad \dots (12)$$

where, $I_{D(P1)}$, $I_{D(N1)}$, $\mu_{(P1)}$, $\mu_{(N1)}$, $V_{DS(P1)}$, $V_{DS(N1)}$, V_{DD}, and R_D, are the drain current in p- channel, drain current in n-channel, mobility in p- channel, mobility in n-channel, drain-source voltage in p- channel, drain-source voltage in n-channel, supply voltage, and drain resistance, respectively, for the transistors in substrate.

The MOSFETs P2 and N2 are at the edges of the diaphragm, and they will form the positive tensile stress (T_e) under pressure. Hence, there will be variations in channel mobilities, drain current, and drain voltage, and therefore, the equations of change in mobilities are given as:

$$\Delta\mu_{(P2)} = -\mu_{(P2)}\pi T_e$$
$$\Delta\mu_{(N2)} = -\mu_{(N2)}\pi T_e \quad \dots (13)$$

Due to changes that are occurring in mobility, the drain current in p-channel and n-channel ($I_{D(P2)}$ & $I_{D(N2)}$), and drain to source voltage in p-channel and n-channel ($V_{DS(P2)}$ & $V_{DS(N2)}$), for P2 and N2 are represented as:

For p-MOSFET:

$$I_{D(P2)} = \{\mu_{(P2)} + \Delta\mu_{(P2)}\}C_{ox}\frac{W}{L}\frac{(V_{GS} - V_t)}{2} = (1 - \pi T_e)I_{D(P1)} \quad \dots (14)$$

$$V_{DS(P2)} = V_{DD} - I_{D(P2)}R_D \quad \dots (15)$$

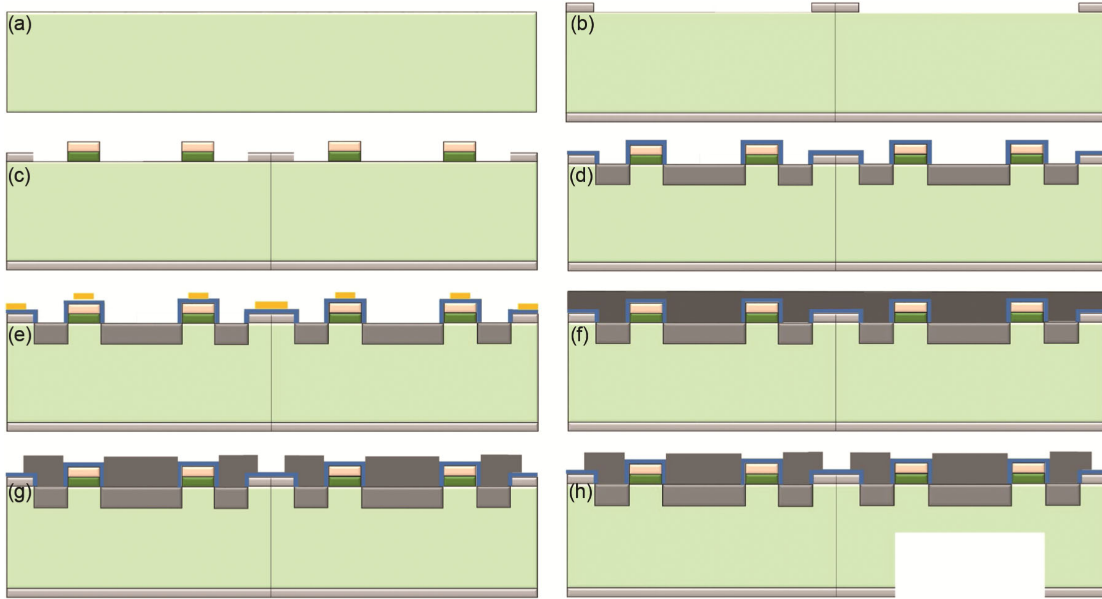

Fig. 4 — Fabrication steps: (a) Silicon wafer (both sides polished), (b) Photolithography (PLG) – 1: Patterning and forming active regions (Mask–1), (c) PLG – 2: Patterning and etching of polysilicon (Mask–2), (d) PLG – 3: Patterning and forming contact vias (Mask–3), (e) PLG – 4: Patterning of metal contact lines and pads (Mask–4), (f) Aluminum deposition, (g) Formation of metal contact line/pads using lift-off process, (h) DRIE etching of silicon from backside

For n-MOSFET:

$$I_{D(N2)} = \{\mu_{(N2)} + \Delta\mu_{(N2)}\}C_{ox}\frac{W}{L}\frac{(V_{GS} - V_t)}{2} = (1 - \pi T_e)I_{D(N1)} \quad \ldots(16)$$

$$V_{DS(N2)} = V_{DD} - I_{D(N2)}R_D \quad \ldots(17)$$

Therefore, the output voltages are found in the drain terminals for both p-MOSFET and n-MOSFET under the applied pressure and are presented as:

$$V_{out} = \left(V_{DS(P1)} - V_{DS(P2)}\right) : \text{For p-MOSFET}$$
$$V_{out} = \left(V_{DS(N1)} - V_{DS(N2)}\right) : \text{For n-MOSFET} \quad \ldots(18)$$

CMOS (integrated p-MOS and n-MOS) CM

The circuit CMOS (integrated p-MOS and n-MOS) has two transistors acting as reference transistors (P1 and N1) and another two transistors (P2 and N2) acting as sensing transistors, and the expressions have been given below:[28]

$$V_{GS1} = V_{DS1} \quad \ldots(19)$$

$$V_{DS1} = \frac{V_{DD} - |V_{Tp}| + V_{Tn}\sqrt{\frac{\mu_{n1}}{\mu_{p1}}}}{1 + \sqrt{\frac{\mu_{n1}}{\mu_{p1}}}} \quad \ldots(20)$$

$$V_{DS2} = \frac{V_{DD} - |V_{Tp}| + V_{Tn}\sqrt{\frac{\mu_{n2}}{\mu_{p2}}}}{1 + \sqrt{\frac{\mu_{n2}}{\mu_{p2}}}} \quad \ldots(21)$$

In the above equations V_{GS1}, V_{Tp}, and V_{Tn} are the gate to source voltage, threshold voltage of PMOS, and threshold voltage of NMOS, respectively. V_{DS1}, μ_{n1}, and μ_{p1} are the drain to source voltages, electron mobility, and hole mobility, respectively, for the transistors P1 and N1. Similarly, V_{DS2}, μ_{n2}, and μ_{p2} are for the transistors P2and N2. The output voltages are obtained across the drain terminals of the MOSFETs (P1, N1 and P2, N2), under the application of pressure and are defined as:

$$V_{out} = (V_{DS1} - V_{DS2}) \quad \ldots(22)$$

Proposed Fabrication Process Flow

The fabrication process flow for the proposed pressure sensors is represented in Fig. 4. It starts with a polished silicon wafer, doped in either boron or phosphorus. The procedure undergoes an initial RCA cleaning process, where DI (deionized) water is used to clean all the apparatus. This cleaning method is used to remove organic and ionic contaminants from the wafer. A SiO_2 layer of 1 µm thick has been grown

at 1100°C using an oxidation technique. Then, followed by the photolithography process, the active regions were defined by the thermal diffusion method. After that, using a dry oxidation process, a thin layer of oxide 85 nm has been developed at 1100°C. Utilizing the LPCVD (low-pressure chemical vapour deposition) technique, a 0.3 µm of thin layer polysilicon has been deposited and formed on the oxidized wafer of silicon. This forms a polysilicon gate of the MOSFET structure. Following the photolithography–2, the phosphorus or boron-doped impurities were introduced through the thermal diffusion process at 1000°C. This creates the sources and drains of the MOSFET structure. The phosphosilicate glass has been formed in n-MOSFET, and the borosilicate glass in p-MOSFET. Then, by using the photolithography–3 and 4 process, the vias, metal contact lines, and pads were patterned to define the regions. An Aluminum layer was deposited in the next step, and metal contact lines were formed using the lift-off process. The DRIE (deep reactive ion etching) process has been utilized for etching out the backside of the wafer to enable the formation of the diaphragm.

Results and Discussions

The Current Mirror integrated Split curved channel MOSFET pressure sensors are designed using the SCL 180 nm CMOS technology. The technology parameters are given in Table 1. The COMSOL Multiphysics finite element analysis software has been utilized to determine the mechanical behavior and piezoresistive response of the pressure sensor. TSpice software has been utilized to obtain the electrical properties of the pressure sensors. The parameters for designing the proposed pressure sensors on respective circular and square diaphragms are given in Table 2.

The dimensions of the circular and square silicon diaphragms are taken as 100 µm diameter and 100 µm sides, respectively, with 2.5 µm for the thicknesses for both the diaphragm structures. The pressure ranging from 0 to 450 kPa has been applied on the

Table 1 — SCL 180 nm CMOS technology parameters

Parameters	Unit	NMOS	PMOS
Minimum channel length, L_{MIN}	µm	0.5	0.5
Gate oxide thickness, t_{OX}	nm	7	7
Oxide capacitance, C_{OX}	fF/µm^2	4.929	4.929
Channel mobility, µ	cm^2/Vs	243	100
Transconductance parameter, μC_{OX}	µA/V^2	119.761	49.291
Threshold voltage, V_{th}	V	0.707	−0.687
Supply voltage, V_{DD}	V	3.3	3.3
Early voltage parameter, V'_A	V/µm	16.740	99.123

Table 2 — Parameters used for designing the proposed pressure sensors

	Split Circular curved channel pressure sensor				Split Square curved channel pressure sensor			
	NMOS	PMOS	CMOS circuit		NMOS	PMOS	CMOS circuit	
			NMOS	PMOS			NMOS	PMOS
A. Parameters used in T Spice for circuit simulation								
Channel dimensions (µm)	Channel length = 10, Channel width = 100, Channel thickness= 0.5							
Reference current (µA)	514		935		514		935	
Drain resistor (Ω)	3250	450	—	—	3210	450	—	—
Gate-to-source voltage (V)	1.617	0.693	1.925	1.375	1.621	0.694	1.925	1.375
B. Parameters used in COMSOL Multiphysics for structural simulation								
Diaphragm dimensions	Diameter = 100 µm, Thickness = 2.5 µm Material = Silicon				Sides = 100 µm, Thickness = 2.5 µm Material = Silicon			
MOSFET piezoresistor (kΩ)	325.689	1928.457	179.042	1060.136	325.689	1928.457	179.042	1060.136
Voltage applied across piezoresistor (V)	167	991	167	991	167	991	167	991
Piezoresistive coefficients (× 10^{-11} Pa^{-1})	N-MOSFET: π_{11} = 102, π_{12} = −53.4, π_{44} = 13.6 P-MOSFET: π_{11} = −6.6, π_{12} = 1.1, π_{44} = −138							
Pressure range	(0 – 450) kPa in steps of 50 kPa							

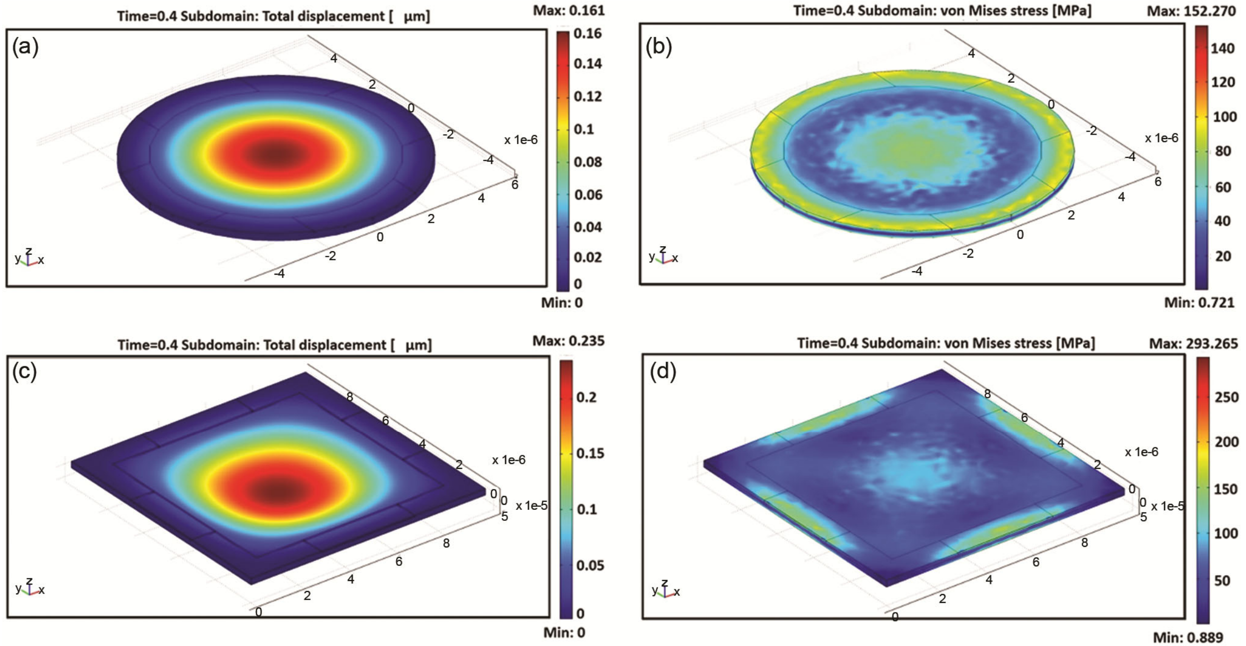

Fig. 5 — For input pressure of 450 kPa: (a) Displacement profile on circular diaphragm, (b) von Mises stress profile on circular diaphragm, (c) Displacement profile on square diaphragm, (d) von Mises stress profile on square diaphragm

diaphragm, due to which deflection occurs, and the maximum displacement occurs at the center of circular and square diaphragms. The displacement and von Mises stress profiles of circular and square diaphragms at 450 kPa applied pressure are shown in Fig. 5. The higher displacement is found to be 0.161 μm for the circular structure and 0.235 μm for the square structure. The maximum stress for the circular diaphragm occurs at the entire periphery of the diaphragm and is found to be 293.265 MPa, and the minimum stress is 0.889 MPa. Similarly, the maximum stress for square diaphragm occurs at the mid-point of the periphery of diaphragm and is found to be 152.270 MPa, and the minimum stress is 0.721 MPa.

The Electric potential and Electric conductivity profiles are shown in Fig. 6. The voltages applied across the piezoresistors of circular and square diaphragms are 167 V for n-MOSFET and 991 V for p-MOSFET. The highest and lowest electric conductivity for the circular diaphragm structures are found to be 0.499 S/m and 0.481 S/m, respectively. Similarly, the highest and lowest electric conductivity for the circular and square diaphragm structures are found to be 0.574 S/m and 0.530 S/m, respectively.

Simulation Results on Variation of Channel Resistance & Channel Mobility in Proposed Pressure Sensors

The variations of Channel Resistance and Channel Mobilities are represented in the graphs shown in Fig. 7. From Fig. 7 (a), it can be observed that for the n-MOS current mirror circuit, the channel resistance increased with increasing pressure. The higher channel resistance is obtained as 331 kΩ for split circular curved n-MOS structure, whereas 333 kΩ for split square curved n-MOS structure. For the p-MOS current mirror circuit, the channel resistance decreased with increasing pressure, as can be observed from Fig. 7 (b). The higher channel resistances are obtained as 1859 kΩ and 1825 kΩ for the split circular and square curved p-MOS structures, respectively. For CMOS (integrated p-MOS & n-MOS), in Fig. 7 (c), the channel resistance for circular is obtained as 1037 kΩ and 181.521 kΩ in p-MOS and n-MOS, respectively. For the square, it is obtained as 1013 kΩ and 182.310 kΩ in p-MOS and n-MOS, respectively.

Similarly, from Fig. 7 (a), (b), and (c), the variation in the carrier mobilities can be observed. The mobilities are decreasing in n-MOS and increasing in p-MOS with an increase in pressure. The channel mobilities for the split circular and square curved n-MOS structures are obtained as 235 cm^2/Vs and 234 cm^2/Vs, respectively. Similarly, for p-MOS, the channel mobilities are obtained as 105 cm^2/Vs and 107 cm^2/Vs for circular and square, respectively. For CMOS (integrated p-MOS & n-MOS), the channel

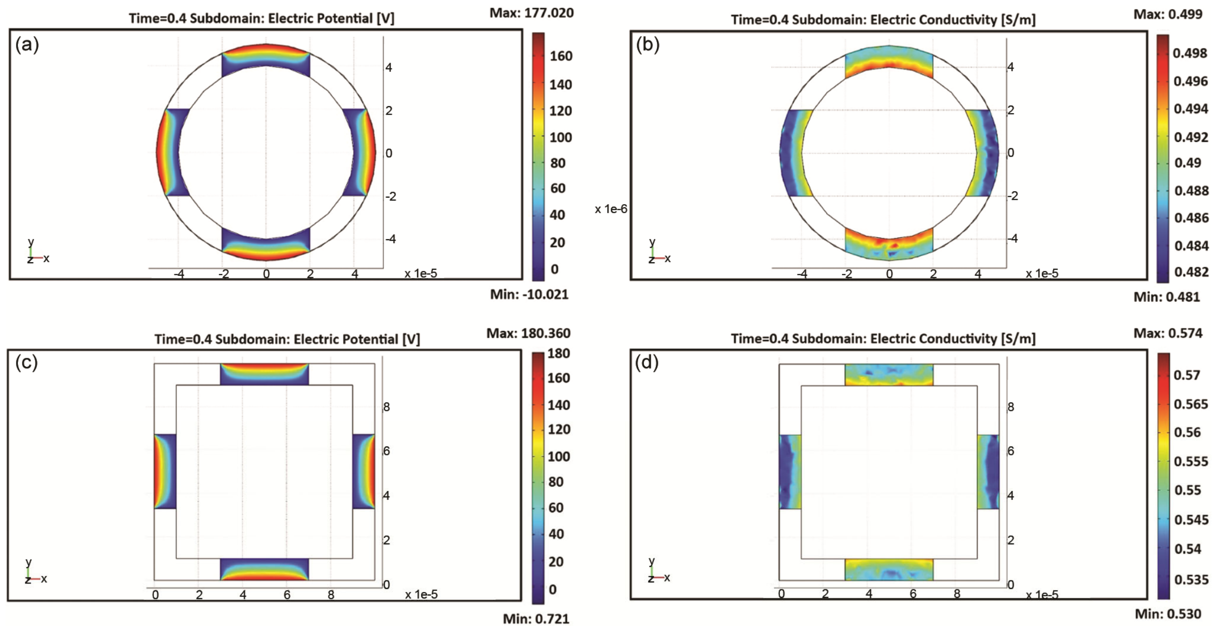

Fig. 6 — For the input pressure of 450 kPa: (a) Electric potential profile on circular diaphragm, (b) Electric conductivity profile on circular diaphragm, (c) Electric potential profile on square diaphragm, (d) Electric conductivity profile on square diaphragm

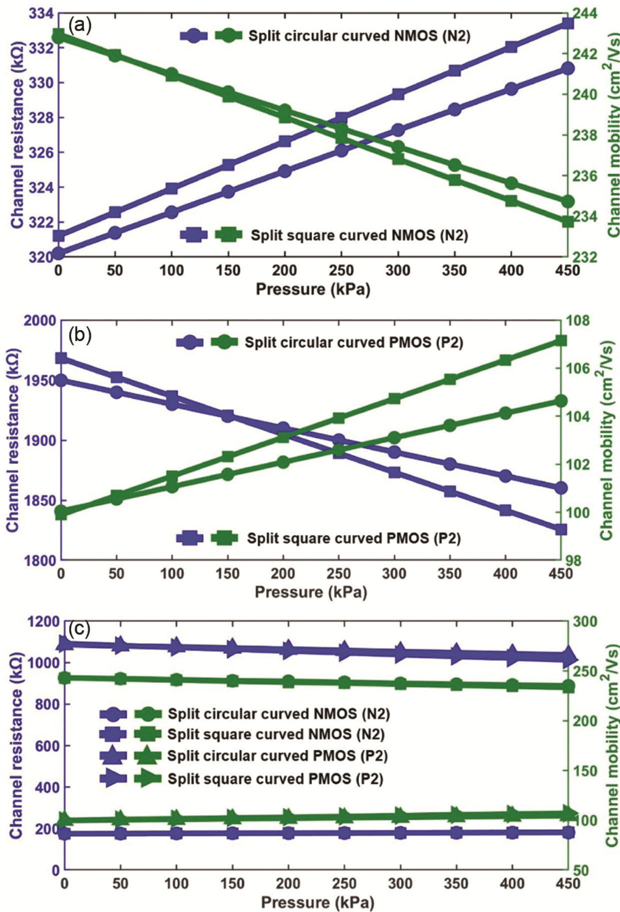

Fig. 7 — Graphs of channel resistance and channel mobility for 0 – 450 kPa pressure range: (a) n-MOS, (b) p-MOS, and (c) CMOS (integrated p-MOS & n-MOS)

mobilities for the circular are obtained as 105 cm^2/Vs and 235 cm^2/Vs in p-MOS and n-MOS, respectively. For the square, it is obtained as 107 cm^2/Vs in p-MOS and 233 cm^2/Vs in n-MOS.

Simulation results on Variation of Drain Current & Drain Voltage in Proposed Pressure Sensors

The graphical representations of the variation in drain current for various applied pressures are shown in Fig. 8 (a), (b), and (c). The maximum drain currents are 500.962 μA and 503.814 μA for the split circular and square curved n-MOS structures, respectively. Similarly, for p-MOS, the drain currents are 531.972 μA and 544.624 μA for circular and square, respectively. For CMOS (integrated p-MOS & n-MOS), the drain current for circular and square are 908.375 μA and 903.950 μA, respectively.

The variation in drain voltage for various applied pressures has also been represented in Fig. 8. It shows that for the higher applied pressure at 450 kPa, the drain voltages are found to be 1.671 V and 1.682 V for the split circular and square curved n-MOS structures, respectively. Similarly, in the split circular and square curved p-MOS structures, the drain voltages are 0.693 V and 0.693 V, respectively — for CMOS (integrated p-MOS & n-MOS), they are found to be 2.098 V and 2.155 V for the respective split circular and square curved CMOS structures.

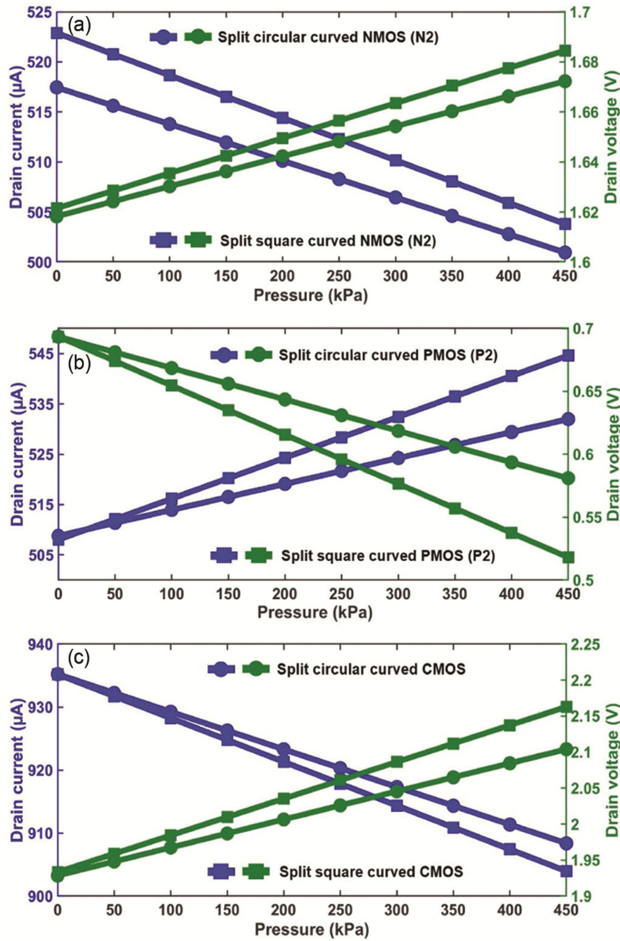

Fig. 8 — Graphs of drain current and drain voltage for 0 – 450 kPa pressure range: (a) n-MOS, (b) p-MOS, and (c) CMOS (integrated p-MOS & n-MOS)

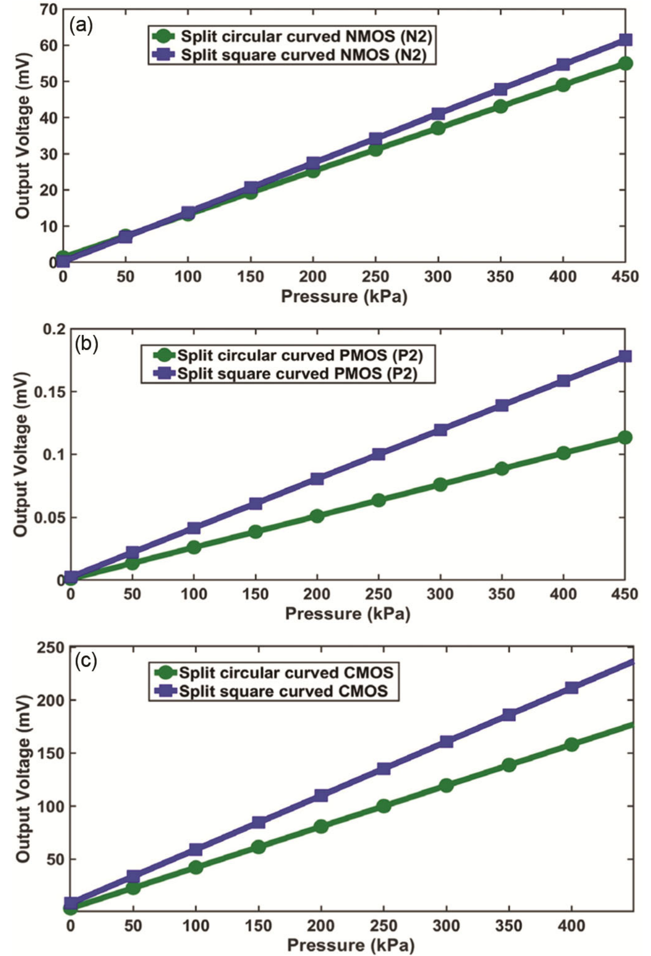

Fig. 9 — Graphs of output voltage for 0 – 450 kPa pressure range: (a) n-MOS, (b) p-MOS, and (c) CMOS (integrated p-MOS & n-MOS)

Simulation Results of Output Voltage in Proposed Pressure Sensors

The output voltage of the proposed n-MOS, p-MOS, and CMOS (integrated p-MOS & n-MOS) current mirrors, individually integrated on the Split circular curved channel pressure sensors and Split square curved channel pressure sensors, has been evaluated and represented in Fig. 9.

The sensitivities for n-MOS, p-MOS, and CMOS (integrated p-MOS & n-MOS) current mirrors, on the Split circular curved channel pressure sensors, are obtained as 122.051, 0.249, and 377.611 mV/MPa, respectively. Similarly, for the Split square curved channel pressure sensors, the sensitivities are obtained as 138.821, 0.401, and 492.250 mV/MPa, respectively. From Table 3, it can be observed that the sensitivity varies for different diaphragm thicknesses. It has been calculated, compared and observed that with the decreasing thickness of diaphragms, the pressure sensors become highly sensitive. A comparison of sensor sensitivity with various piezoresistive pressure sensor designs reported in recent literature is presented in Table 4. The pressure sensors proposed in this work may be used for various applications, as listed in Table 5, within a pressure range of 0–500 kPa.

Temperature Effects on Current Mirror Integrated Split Curved Channel MOSFET Pressure Sensor

This section explains the influence of temperatures on the proposed silicon-based pressure sensors. Here, the concept of temperature compensation has been utilized to study and observe the sensitivities at different temperatures for the proposed pressure sensors. The current mirror circuits are the most commonly used biasing circuits that provide steady currents to the integrated circuits (ICs).[22] It is one of the simplest and most fundamental circuits, where the

Table 3 — Sensitivities of the proposed pressure sensors for different diaphragm thicknesses

Diaphragm thickness	Sensitivities for Split circular curved channel pressure sensor in mV/MPa		
	NMOS	PMOS	CMOS
2.5	122.051	0.249	377.611
5	33.270	0.064	120.040
10	8.541	0.017	32.960
Diaphragm thickness	Sensitivities for Split square curved channel pressure sensor in mV/MPa		
2.5	138.821	0.401	492.250
5	37.870	0.108	161.571
10	9.570	0.025	44.130

Table 4 — Comparison of sensor sensitivity with various piezoresistive pressure sensor design available in literature

Reported works on various piezoresistive pressure sensors	Sensitivity
MOSFET-based rectangular-shaped piezoresistor[27]	782 mV/MPa 633 mV/MPa
Piezoresistors are arranged on each side of the square diaphragm, making it in series and strip-shaped[36]	7.74 mV/V/MPa
S-shaped piezoresistor piezoresistive pressure sensor[37]	0.802 mV/V/MPa
Grapheme piezoresistive pressure sensor integrating zig-zag shaped piezoresistors[40]	609.16 mV/MPa
A piezoresistive pressure sensor for n-type Silicon diaphragm in Meander-shaped piezoresistor[41]	2360 mV/MPa 1640 mV/MPa
Split circular curved shape piezoresistor	122.051, 0.249, 377.611 (mV/MPa)
Split square curved shape piezoresistor	138.821, 0.401, 492.250(mV/MPa)

Table 5 — Existing applications of pressure sensors for 0–500 kPa input range

Application Area	Typical use of pressure sensor 0–500 kPa Range	Market available pressure sensors
Automotive and embedded control systems	Air, gas, and moderate fluid pressure sensing in electronically controlled systems	NXP Semiconductors, Differential Integrated Pressure Sensor (0 to 500 kPa), MPX5500D [https://www.nxp.com/docs/en/data-sheet/MPX5500.pdf]
Industrial process monitoring	Pressure measurement in compressed air lines, pumps, process gas lines, and utility pressure monitoring	NXP Semiconductors, MPXV5100: Differential, Gauge and Absolute Integrated Pressure Sensor (0 to 115 kPa) [https://www.nxp.com/docs/en/data-sheet/MPX5100.pdf]
HVAC and ventilation systems	Filter monitoring, duct pressure, airflow verification, fan/blower monitoring, heat exchanger pressure drop	WIKAA2G-40 [https://www.wika.com/en-in/a2g_40.WIKA]
Clean room and laboratory pressure control	Positive / negative pressure control, room isolation, laboratory pressure balancing	WIKAA2G-500 [https://www.wika.com/en-in/a2g_500.WIKA]
Medical and healthcare devices	Ventilator pressure monitoring, patient monitoring, respiratory flow / gas pressure sensing, suction / pump systems	NXP Semiconductors, MPXx4006 [https://www.nxp.com/docs/en/data-sheet/MPXV4006.pdf]
Water and fluid management systems	Water pipeline pressure, pump discharge/suction monitoring, filtration systems, leak detection	NXP Semiconductors, MPX5500, and WIKA A2G-500
Consumer appliances and smart systems	Washing machines, air handling units, smart pumps, appliance pressure control, beverage / fluid systems	NXP Semiconductors, MPX5500 series [https://www.nxp.com/docs/en/data-sheet/MPX5500.pdf]
Research and laboratory instrumentation	Gas line pressure, pressure chamber testing, microfluidics, sensor calibration, diaphragm characterization	NXP Semiconductors, MPX5500DP and related MEMS pressure sensor families [https://www.nxp.com/docs/en/data-sheet/MPX5500.pdf]

Table 6 — Pressure sensitivities at different temperatures for the proposed pressure sensors

Temperatures (degree Celsius)	Pressure sensitivities for Split circular curved channel pressure sensor in mV/MPa			Pressure sensitivities for Split square curved channel pressure sensor in mV/MPa		
	NMOS	PMOS	CMOS	NMOS	PMOS	CMOS
0°C	112	0.009	349	136	0.015	460.210
27°C (room temp.)	122.051	0.249	377.611	138.821	0.401	492.250
50°C	137	4.066	414	141	6.545	531
75°C	172	19.085	458	147	30.442	574
100°C	184	24.368	484	191	41.222	617

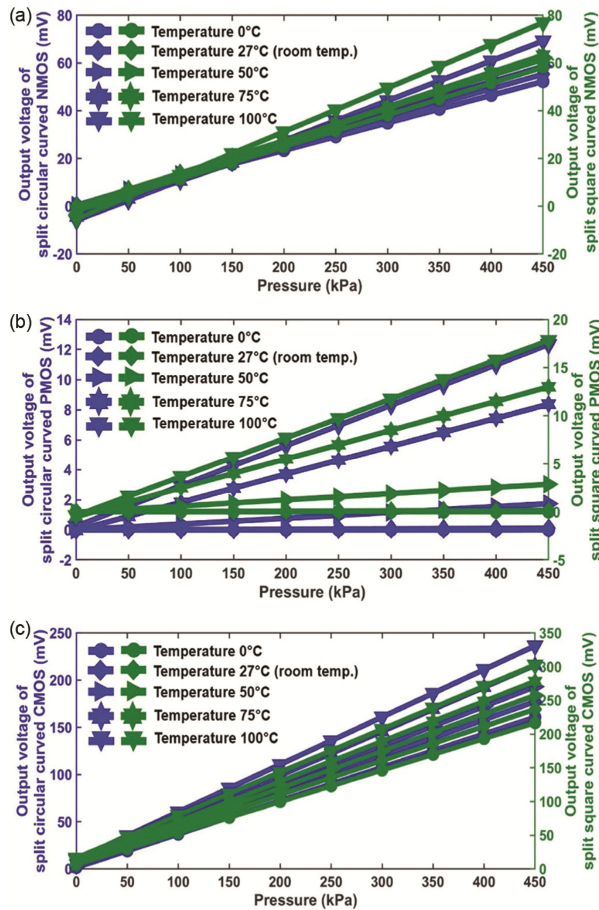

Fig. 10 — Graphs of output voltage of split circular and square curved channel MOSFET pressure sensors for different temperatures: (a) n-MOS, (b) p-MOS, and (c) CMOS (integrated p-MOS & n-MOS)

constant current references are generated on the input transistors and imitate the same current in the output transistors of circuits.[38,39] TSpice software has been utilized to study the effects of temperatures for n-MOS, p-MOS, and CMOS (integrated p-MOS & n-MOS) circuits that are individually integrated in each circular and square diaphragm. The operating temperatures are taken at 0°, 27°, 50°, 75°, and 100°C for all the proposed pressure sensors.

The simulation result shows that under zero pressure, with the changing temperatures, the changes in the electrical properties of MOSFET transistors would be identical. Therefore, the drain terminals of the MOSFETs could have equal voltages, resulting in zero output voltages for the changing temperatures. However, under the applied input pressure, there will be change in mobilities, drain current, and drain voltages, due to which there will be a change in output voltages. The sensitivities in each given temperature have been found, and it has been observed that with the increase in temperature, the sensitivity increases.

The variation in output voltage for the given different temperature ranges for various applied pressures from 0 kPa to 450 kPa has been represented graphically in Fig. 10. The pressure sensitivities in mV/MPa, for the proposed pressure sensors in circular and square structures for different temperature ranges are shown in Table 6. The sensitivities vary in both split circular and square structured pressure sensors. Among which, the CMOS (integrated p-MOS & n-MOS) is showing the better sensitivities for both diaphragm geometries.

Conclusions

The paper is a detailed study on the simulation of the current mirror integrated split curved channel MOSFET pressure sensor. The n-MOS, p-MOS, and CMOS (integrated p-MOS and n-MOS) current mirrors, each integrating on Split circular and square curved channel structures, were found to have better sensitivities. Also, the pressure sensors function beyond the room temperature and are capable of operating at higher temperatures. Therefore, these proposed pressure sensors have the potential to emerge as an alternative to the conventional Wheatstone bridge configured pressure sensors. Also, this design technology allows the pressure sensors to enable the monolithic integration of pressure sensors in a single-chip package, and is capable of

CMOS fabrication process. They are cost-agnostic, space-saving, and provide enhanced sensitivity. Thus, these pressure sensors can be deployed in the foreseeable future across medical, industrial, and commercial applications.

Acknowledgment

This work was supported by the Department of Science and Technology, Government of India [Project grant number: DST/TDT/DDP-36/2021]. The authors would also like to acknowledge the use of a high end desktop computer system obtained under the project grant [ISRO/RES/3/807/18-19] for carrying out few simulations reported in this paper. The authors have no conflict of interest to declare. All authors have participated in the work carried out in this paper.

References

1 Jena S & Gupta A, Review on pressure sensors: a perspective from mechanical to micro-electro-mechanical systems, *Sensor Review*, **41(3)** (2021) 320–329, doi:10.1108/SR-03-2021-0106.

2 Bogue R, MEMS sensors: past, present and future, *Sensor Review*, **27(1)** (2007) 7–13, doi:10.1108/02602 280710729068.

3 Lee Y C, Hsieh M L, Lin P S, Yang C H, Yeh S K, Do T T & Fang W, CMOS-MEMS technologies for the applications of environment sensors and environment sensing hubs, *J Micromech Microeng*, **31(7)** (2021) doi:10.1088/ 1361-6439/ac05146439/ac0514.

4 Qu H, CMOS MEMS fabrication technologies and devices, *Micromachines*, **7(1)** (2016) 14, doi:10.3390/ mi7010014.

5 Fang W, Li S S, Cheng C L, Chang C I, Chen W C, Liu Y C, Tsai M H & Sun C, CMOS MEMS: A key technology towards the More than Moore era, in *Int Conf Solid-State Sens Actuators Microsystems (TRANSDUCERS & EUROSENSORS XXVII)* (Barcelona, Spain) 16–20 June 2013, 2513–2518, doi:10.1109/Transducers.2013.6627317.

6 Song P, Ma Z, Ma J, Yang L, Wei J, Zhao Y, Zhang M, Yang F & Wang X, Recent Progress of Miniature MEMS Pressure Sensors, *Micromachines*, **11(1)** (2020) 56, doi:10.3390/mi11010056.

7 Han X, Huang M, Wu Z, Gao Y, Xia Y, Yang P, Fan S, Lu X, Yang X, Liang L, Su W, Wang L, Cui Z, Zhao Y, Li Z, Zhao L & Jiang Z, Advances in high-performance MEMS pressure sensors: Design, fabrication, and packaging, *Microsyst Nanoeng*, **9(1)** (2023) 156, doi:10.1038/s41378-023-00620-1.

8 Song P, Ma Z, Ma J, Yang L, Wei J, Zhao Y, Zhang M, Yang F & Wang X, Recent progress of miniature MEMS pressure sensors, *Micromachines*, **11(1)** (2020) 56, doi:10.3390/mi11010056.

9 Chowdhury A H, Jafarizadeh B, Baboukani A R, Pala N & Wang C, Monitoring and analysis of cardiovascular pulse waveforms using flexible capacitive and piezoresistive pressure sensors and machine learning perspective, *Biosens Bioelectron*, **237** (2023) 115449, doi:10.1016/j.bios.2023.115449.

10 Zhang T, Liu N, Xu J, Liu Z, Zhou Y, Yang Y, Li S, Huang Y & Jiang S, Flexible electronics for cardiovascular healthcare monitoring, *The Innovation*, **4(5)** (2023) 100485, doi:10.1016/j.xinn.2023.100485.

11 Bao M H, *Analysis and Design Principles of MEMS Devices*, **1st edn**, (Elsevier, Amsterdam) 2005.

12 Liu C, *Foundations of MEMS*, **2nd edn**, (Pearson Education, India) 2012.

13 Aryafar M, Hamedi M & Ganjeh M M, A novel temperature compensated piezoresistive pressure sensor, *Measurement*, **63** (2015) 25–29, doi:10.1016/j.measurement.2014.11.032.

14 Yao Z, Liang T, Jia P, Hong Y, Qi L, Lei C, Zhang B, Li W, Zhang D & Xiong J, Passive resistor temperature compensation for a high-temperature piezoresistive pressure sensor, *Sensors*, **16(7)** (2016) 1142, doi:10.3390/s16071142.

15 Yao Z, Liang T, Jia P, Hong Y, Qi L, Lei C, Zhang B & Xiong J, A high-temperature piezoresistive pressure sensor with an integrated signal-conditioning circuit, *Sensors*, **16(6)** (2016) 913, doi:10.3390/s16060913.

16 Kim H, Jeong Y G & Chun K, Improvement of the linearity of a capacitive pressure sensor using an interdigitated electrode structure, *Sensors and Actuators A: Physical*, **62(1)** (1997) 586–590, doi:10.1016/S0924-4247(97)01591-4.

17 Ji J, Cho S T, Zhang Y, Najafi K & Wise K D, An ultraminiature CMOS pressure sensor for a multiplexed cardiovascular catheter, *IEEE Transactions on Electron Devices*, **39(10)** (1992) 2260–2267, doi:10.1109/16.158797.

18 Wang Y & Chodavarapu V P, Differential wide temperature range CMOS interface circuit for capacitive MEMS pressure sensors, *Sensors*, **15(2)** (2015) 4253–4263, doi:10.3390/s150204253.

19 Baptista F G, Budoya D E, de Almeida V A D & Ulson J A C, An experimental study on the effect of temperature on piezoelectric sensors for impedance-based structural health monitoring, *Sensors*, **14(1)** (2014) 1208–1227, doi:10.3390/s140101208.

20 Hopkins M B & Lee P, High frequency amplifiers for piezoelectric sensors noise analysis and reduction techniques, in *IEEE Int Instrum Meas Technol Conf (I2MTC) Proc* (Pisa, Italy) 11–14 May 2015, 893–898, doi:10.1109/I2MTC.2015.7151387.

21 McGrath M J & Scanaill C N, Sensing and sensor fundamentals, in *Sensor Technologies*, Springer Nature Publications (Apress, Berkeley, CA) 2013, 15–38, doi:10.1007/978-1-4302-6014-1_2.

22 Sedra A S & Smith K C, *Microelectronic Circuits: Theory and Applications* (Oxford University Press, New York) 2017.

23 Shekhawat G, Tark S H & Dravid V P, MOSFET-embedded microcantilevers for measuring deflection in biomolecular sensors, *Science*, **311(5767)** (2006) 1592–1595, doi:10.1126/science.1122588.

24 Shekhawat G & Dravid V P, Microelectronics meets biomedicine: Integrated MOSFET-embedded cantilever sensor and diagnostics system, in *Int Workshop Phys Semicond Devices* (Mumbai, India) 16–20 December 2007, 693–694, doi:10.1109/IWPSD.2007.4472614.

25 Rathore P K & Panwar B S, Design and optimization of a CMOS-MEMS integrated current mirror sensing based

MOSFET embedded pressure sensor, in *IEEE Int Conf Control Appl (CCA)* (Hyderabad, India) 28–30 Aug 2013, 443–448, doi:10.1109/CCA.2013.6662789.

26 Rathore P K, Panwar B S & Akhtar J, A novel CMOS-MEMS integrated pressure sensing structure based on current mirror sensing technique, *Microelectronics International*, **32(2)** (2015) 81–95, doi:10.1108/MI-11-2014-0048.

27 Kumar S, Rathore P K & Akhtar J, A comparative study on p- and n-channel MOSFET embedded pressure sensing structures integrated with current mirror readout circuitry, in *IEEE Students' Conference on Electrical, Electronics and Computer Science (SCEECS)* (Bhopal, India) 5–6 March 2016, 1–4, doi:10.1109/SCEECS.2016.7509262.

28 Kumar S, Ropmay G D, Rathore P K, Rangababu P & Akhtar J, Design and simulation of a novel dual current mirror based CMOS-MEMS integrated pressure sensor, *IET Sci Meas Technol*, **15(3)** (2021) 268–278, doi:10.1049/smt2.12028.

29 Rathore P K, Panwar B S & Pandya H J, High sensitivity square ring channel shaped MOSFET embedded pressure sensor integrated with a current mirror readout circuitry, in *IEEE SENSORS* (Baltimore, MD, USA) 3–6 November 2013, 1–4, doi:10.1109/ICSENS.2013.6688395

30 Rathore P K & Panwar B S, CMOS-MEMS integrated MOSFET embedded bridge structure based pressure sensor, in *Annual IEEE India Conf (INDICON)* (Mumbai, India) 13–15 December 2013, 1–6, doi:10.1109/ INDCON. 2013.6725926.

31 Rathore P K & Panwar B S, High sensitivity CMOS pressure sensor using ring channel shaped MOSFET embedded sensing, in *IEEE Int Conf Electron Comput Commun Technol (CONECCT)* (Bangalore, India) 6–7 January 2014, 1–5, doi:10.1109/CONECCT.2014.6740290.

32 Tetseo M, Gogoi K, Kumar S, Kumar G, Rangababu P, Singh A P & Rathore P K, A conceptual study on novel current mirror integrated cantilever (CMIC) mass sensor for micro-gram (μg) range sensing applications, *Microsyst Technol*, **30(2)** (2024) 433–442, doi:10.1007/s00542-023-05594-8.

33 Gogoi K, Tetseo M, Kumar G, Rathore P K, Kumar S, Rangababu P, Singh J & Panwar B S, A conceptual and simulation study on curved MOSFET-based current mirror integrated pressure sensors (CM-CMIPS), *Indian J Eng Mater Sci*, **32(1)** (2025) 32–41, doi:10.56042/ijems. v32i01.12111.

34 Kumar S, Ropmay G D, Rathore P K, Rangababu P & Akhtar J, Fabrication and testing of PMOS current mirror-integrated MEMS pressure transducer, *Sensor Review*, **40(2)** (2020) 141–151, doi:10.1108/SR-07-2019-01822.

35 Kumar S, Rathore P K, Panwar B S & Akhtar J, Development of a current mirror-integrated pressure sensor using CMOS-MEMS cofabrication techniques, *Microelectron Int*, **35(4)** (2018) 203–210, doi:10.1108/MI-05-2017-00222.

36 Farhath M & Samad M F, Design and simulation of a high sensitive stripped-shaped piezoresistive pressure sensor, *J Comput Electron*, **19(1)** (2020) 310–320, doi:10.1007/s10825-019-01429-w.

37 Li T, Xue H & Wang W, A high-pressure sensor with high linearity with s-shaped piezoresistors, *IEEE Sensors J*, **23(2)** (2023) 1052–1059, doi:10.1109/JSEN.2022.3220634.

38 Wada K, Takano M & Sekine K, Analysis on temperature coefficient of a low-voltage current mirror, in *IEEE Faible Tension Faible Consommation* (Paris, France) 20–21 June 2013, 1–4, doi:10.1109/FTFC.2013.6577777.

39 Cesar W V C, Thainann H P C, Gabriel A F S, Robson L M & Dalton M C, A review of CMOS current references, *J Integr Circuits Syst*, **17(1)** (2022), doi:10.29292/jics.v17i1.592.

40 Nag M, Kumar A & Pratap B, A novel graphene pressure sensor with zig–zag shaped piezoresistors for maximum strain coverage for enhancing the sensitivity of the pressure sensor, *Int J Simul Multidiscipt Des Optim*, **12** (2021), doi:10.1051/smdo/2021013.

41 Meti S, Balavalad K B, Katageri A C & Sheeparamatti B G, Sensitivity enhancement of piezoresistive pressure sensor with meander shape piezoresistor, in *Int Conf Energy Efficient Technol Sustain (ICEETS)* (Nagercoil, India) 7–8 April 2016, 890–895, doi:10.1109/ICEETS. 2016.7583874.